High Performance Circuit Pastes for Solid Oxide Fuel Cell Applications

Genzhi Hu,[1] Quan Zhou,[1] Aishwarya Bhatlawande,[2] Jiyun Park,[1] Robert Termuhlen,[3] Yuxi Ma,[1] Thomas R. Bieler,[1] Hui-Chia Yu,[3] Yue Qi,[1] Timothy Hogan,[2] and Jason D. Nicholas[1]

1 Chemical Engineering and Materials Science Department, Michigan State University
2 Electrical and Computer Engineering Department, Michigan State University
3 Computational Mathematics, Science and Engineering Department, Michigan State University

Funded by the Department of Energy Solid Oxide Fuel Cell Core Technology Program through Agreement Number DE-FE-0031672

July 2020

Outline

- **Background and Motivation**
  - Porous Ni Can Promote Ag Wetting on Different Substrates
- **Experiments**
- **Results and Discussion**
  - The Electrical Performance
  - The Mechanical Performance
  - Ag Wetting Molecular Dynamics Simulation and Optimal Pattern Calculation
  - Nickel Phase Sintering Simulation
- **Conclusions**

Nickel Interlayers Can Be Used to Improve the Wetting and Spreading of Silver on a Variety of Ceramic Substrates

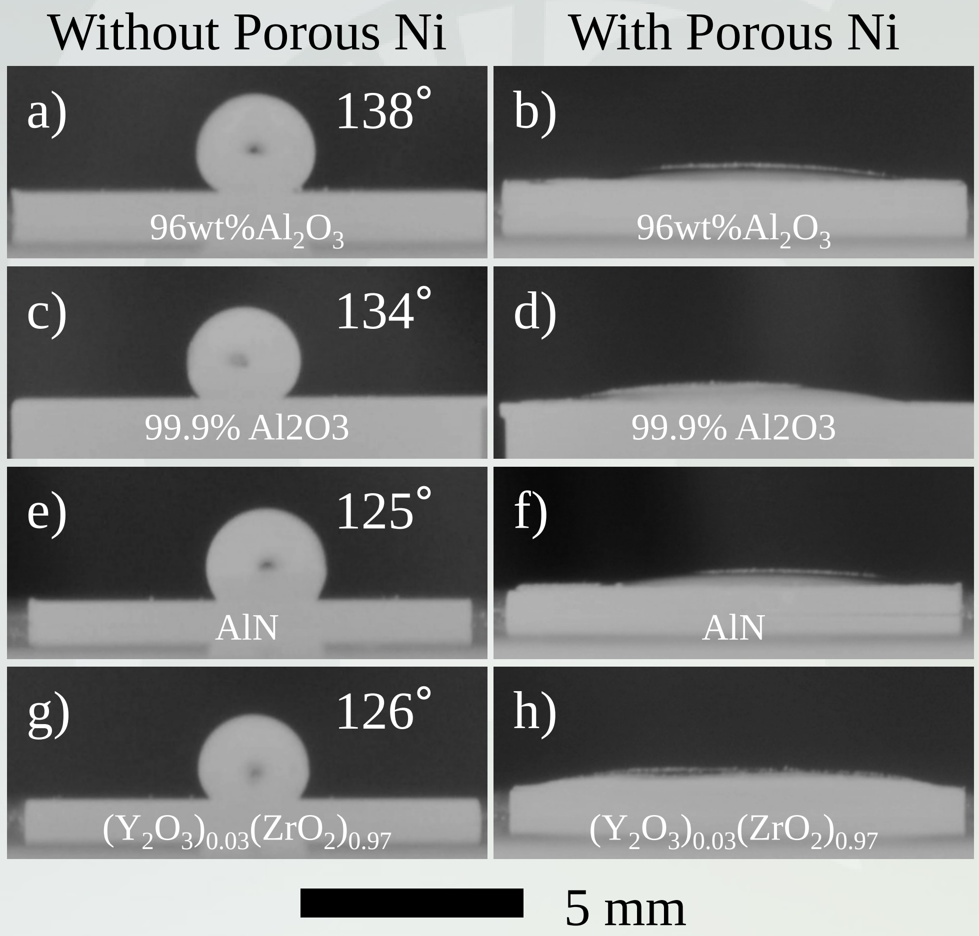

Hu *et al.*, Patterned Porous Nickel Interlayers for Enhanced Silver Wetting, Spreading and Adhesion on Ceramic Substrates, In Preparation, 2020

Outline

- **Background and Motivation**
  - Porous Ni Can Promote Ag Wetting on Different Substrates
- **Experiments**
- **Results and Discussion**
  - The Electrical Performance
  - The Mechanical Performance
  - Ag Wetting Molecular Dynamics Simulation and Optimal Pattern Calculation
  - Nickel Phase Sintering Simulation
- **Conclusions**

Nickel Interlayers Can Also Be Used to Direct the Wetting and Spreading of Silver on a Variety of Ceramic Substrates

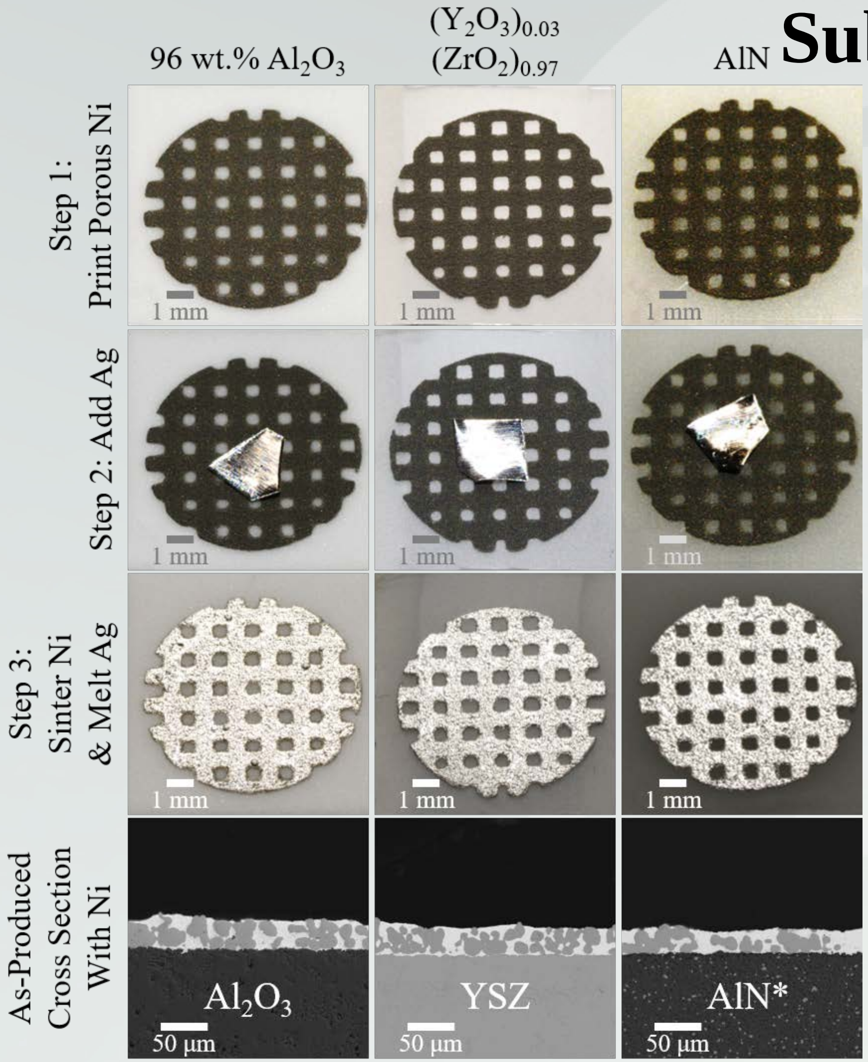

Plan and cross-sectional views of Ag-Ni circuits produced using a 3 step process:

1. Print nickel pastes on the substrate
2. Add a piece of Ag foil
3. Heat to 850℃ for 2 hours in Ar with carbon as an oxygen getter to sinter the Ni and then hold at ~1000 ℃ for 30 minutes to melt the Ag.

Hu *et al.*, Patterned Porous Nickel Interlayers for Enhanced Silver Wetting, Spreading and Adhesion on Ceramic Substrates, In Preparation, 2020

Ag-Ni Circuit Fabrication

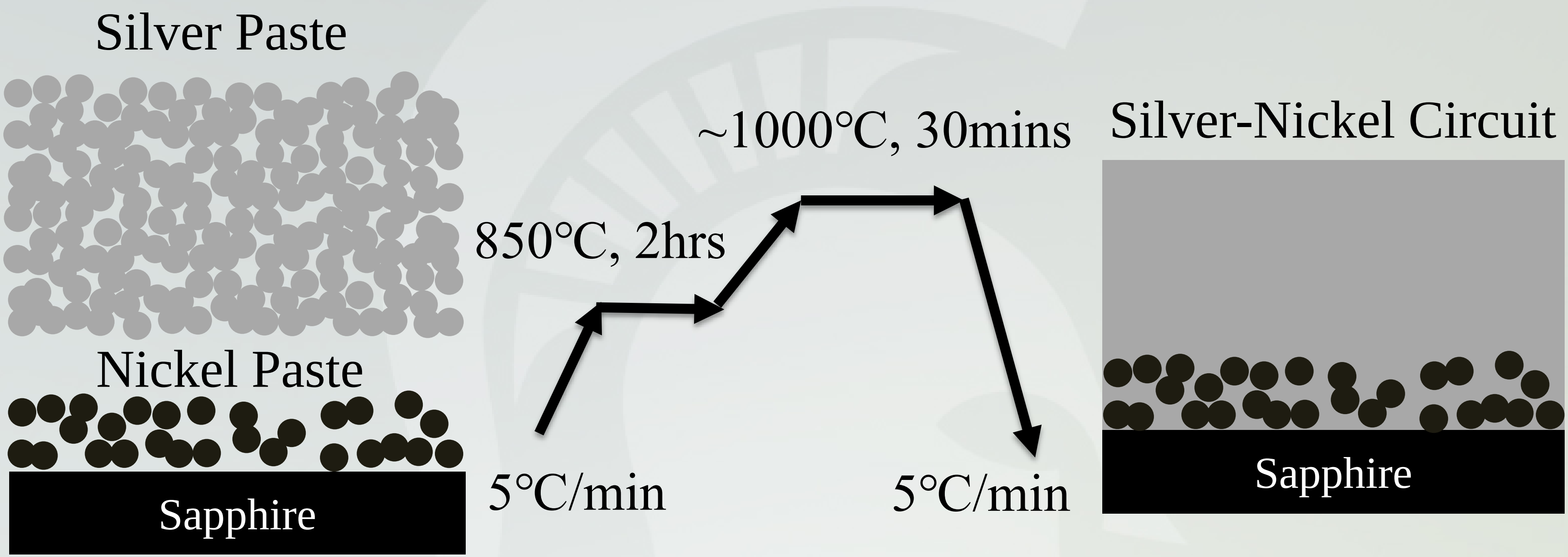

Ar Flow at 20 sccm

Intricate Ag-Ni Circuit Patterns Can Be Produced by Printing and Melting Ag on Screen Printed Ni Inks

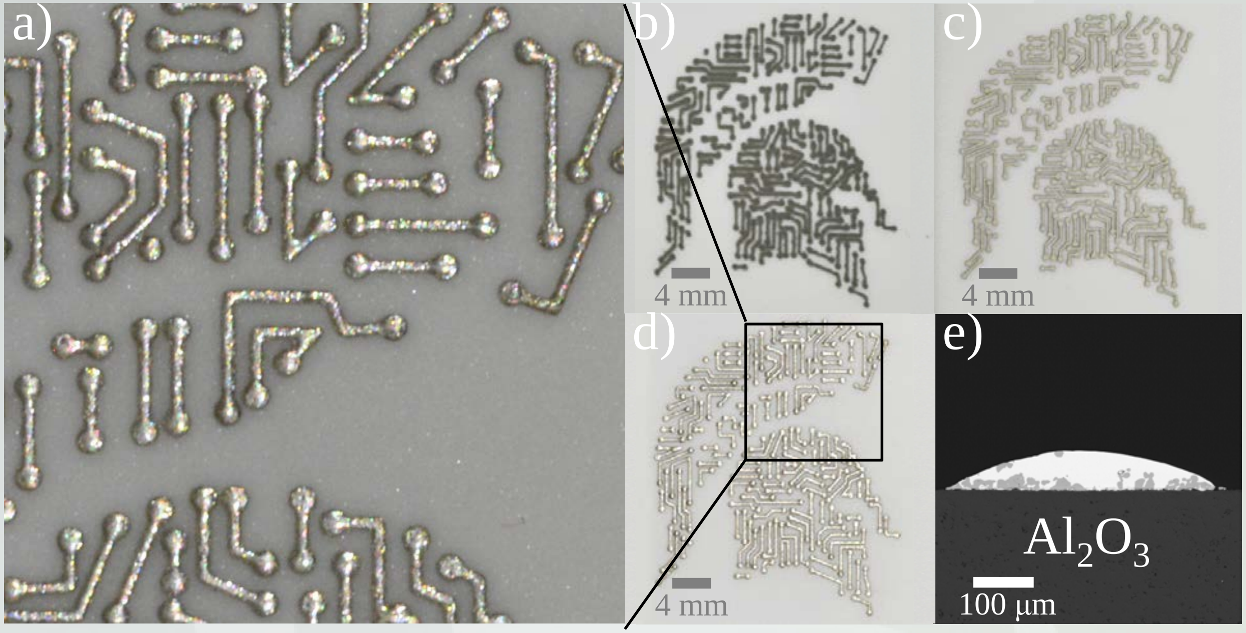

Intricate circuit pattern Figure (a) produced by:
Step 1, Figure (b): Print Ni paste on the substrate
Step 2, Figure (c): Print Ag paste overtop the Ni paste pattern
Step 3, Figure (d): Heat to 850°C for 2 hours in Ar with carbon as an oxygen getter to sinter the Ni and then hold at ~1000 °C for 30 minutes to melt Ag to produce the X-Section in Figure 1(e).

Hu *et al.*, Patterned Porous Nickel Interlayers for Enhanced Silver Wetting, Spreading and Adhesion on Ceramic Substrates, In Preparation, 2020

Outline

- **Background and Motivation**
  - Porous Ni Can Promote Ag Wetting on Different Substrates
- **Experiments**
- **Results and Discussion**
  - The Electrical Performance
  - The Mechanical Performance
  - Ag Wetting Molecular Dynamics Simulation and Optimal Pattern Calculation
  - Nickel Phase Sintering Simulation
- **Conclusions**

The Sheet Resistivity Was Measured in a Van der Pauw Configuration

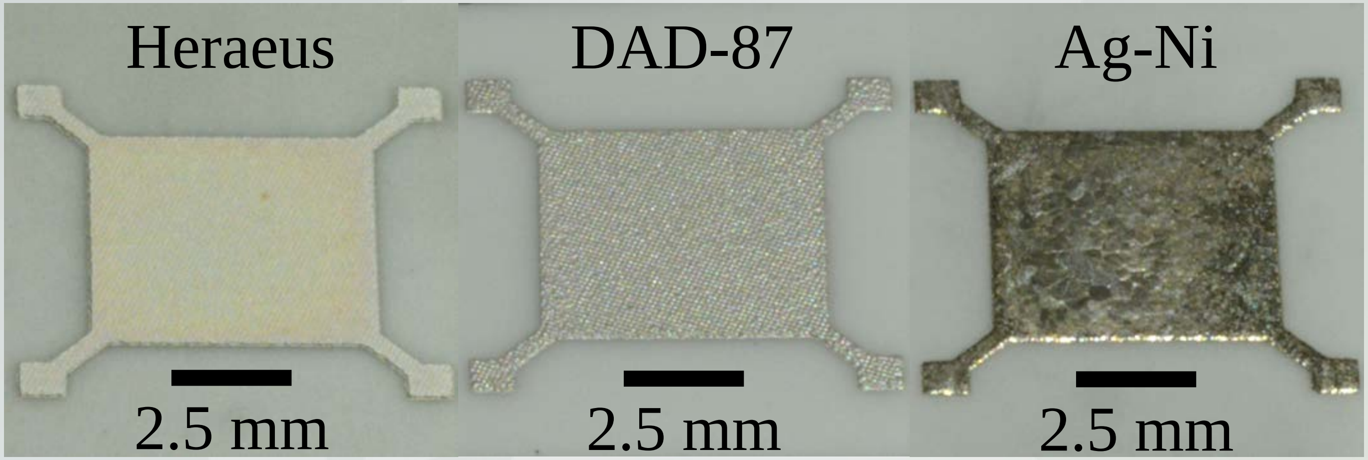

The plan view of as-produced sheet resistivity measurement samples produced by Heraeus C8710, DAD-87 and Ag-Ni

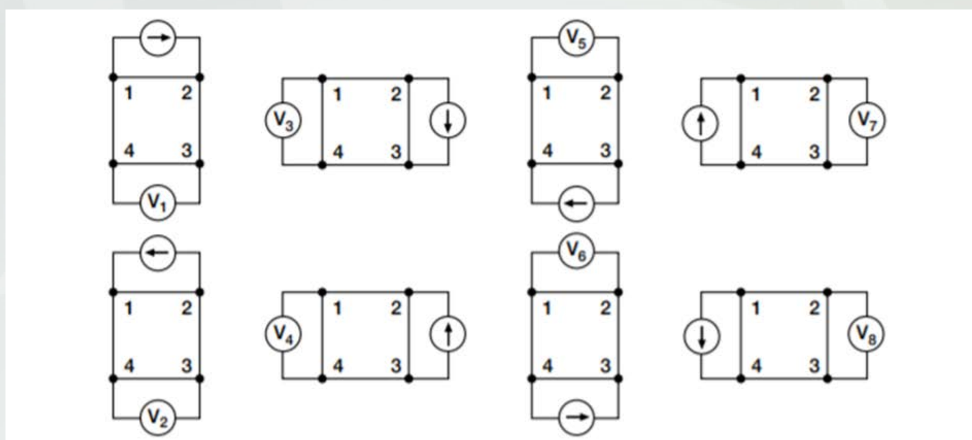

Van der Pauw resistivity measurement configurations

Kim *et al.*, Microelectron. Eng(2014)

The As-Produced Ag-Ni Circuit Has Lower Resistivity than Commercial Ag Pastes. After Annealing in Air, the Resistivity Is Still Comparable to Pure Ag

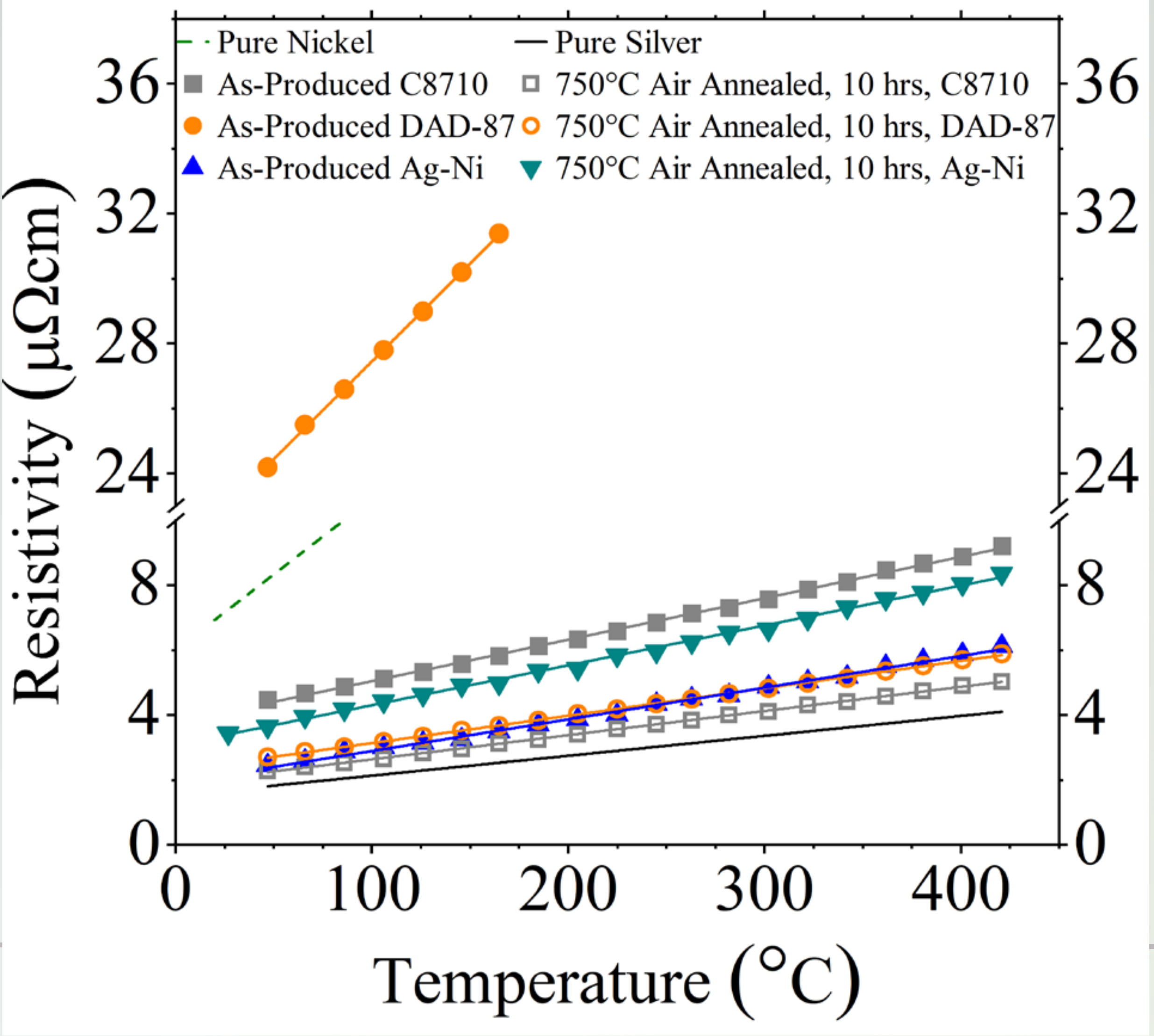

The Lower Resistivity of Ag-Ni than Commercial Ag Pastes Results from the Dense Microstructure

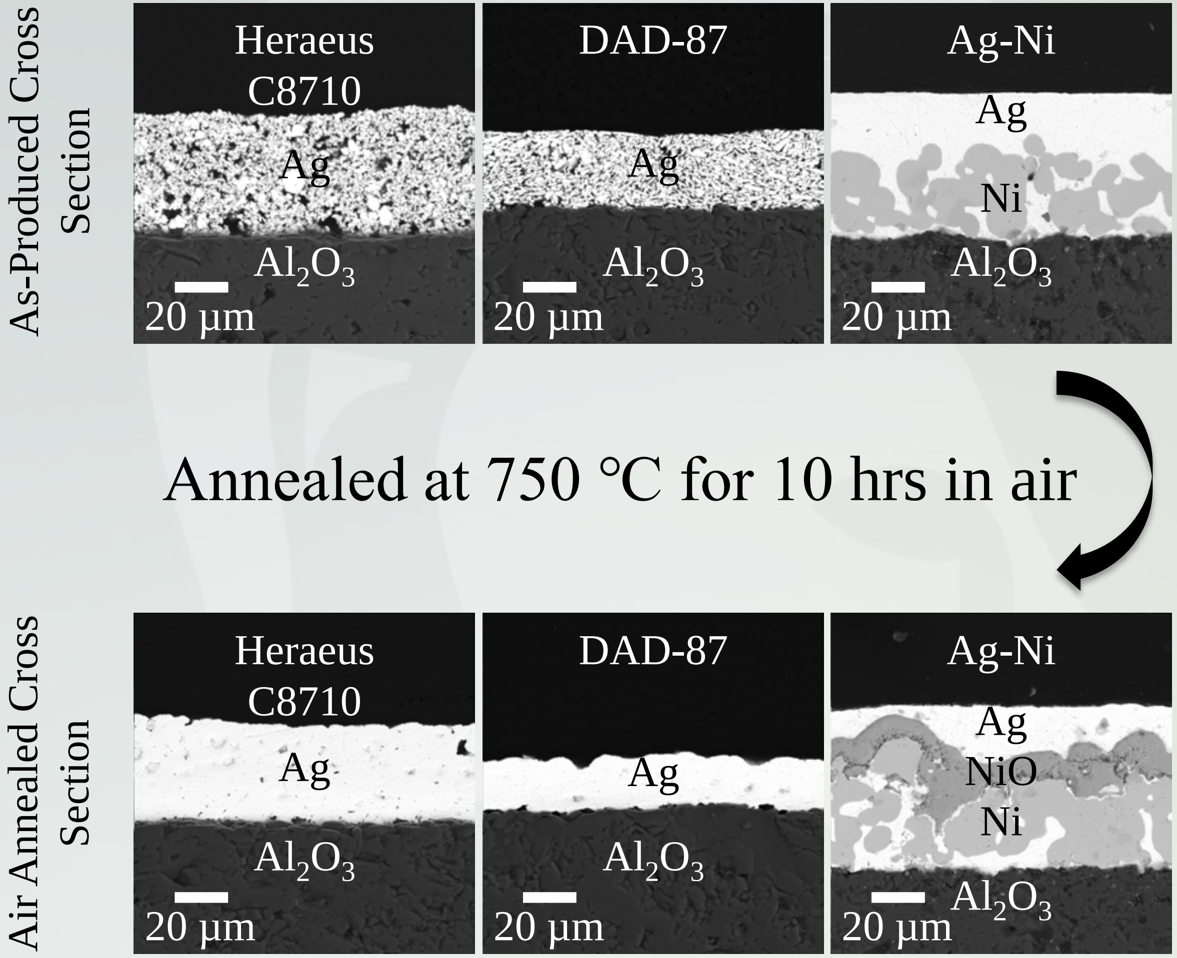

The Contact Resistivity Was Measured by 4-Wire Measurement Technique

Heraeus DAD-87 Ag-Ni

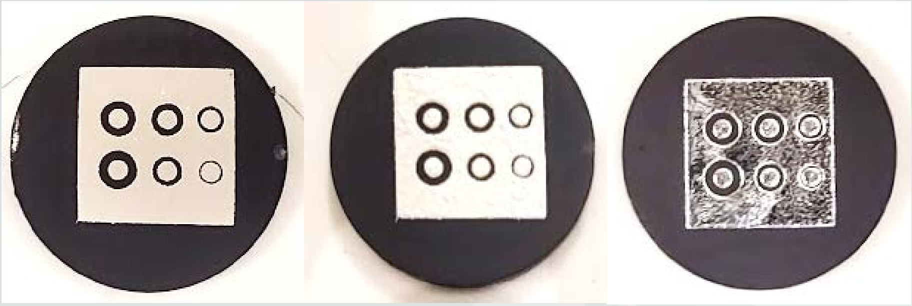

2.5 mm

The plan view of as-produced contact resistivity measurement samples produced by Heraeus C8710, DAD-87 and Ag-Ni on $(La_{0.8}Sr_{0.2})_{0.98}MnO_3$

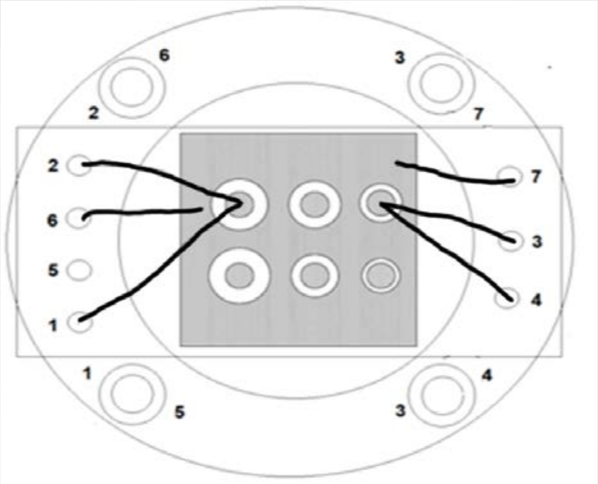

The wire connection illustration

Marlow *et al.*, Solid-State Electrons(1982)
Keithley, "Low Level Measurements Handbook - 7 th Edition.", Tektronix, 2016.

The Ag-Ni Circuit Has Low Contact Resistivity on Lanthanum Strontium Manganite Substrates

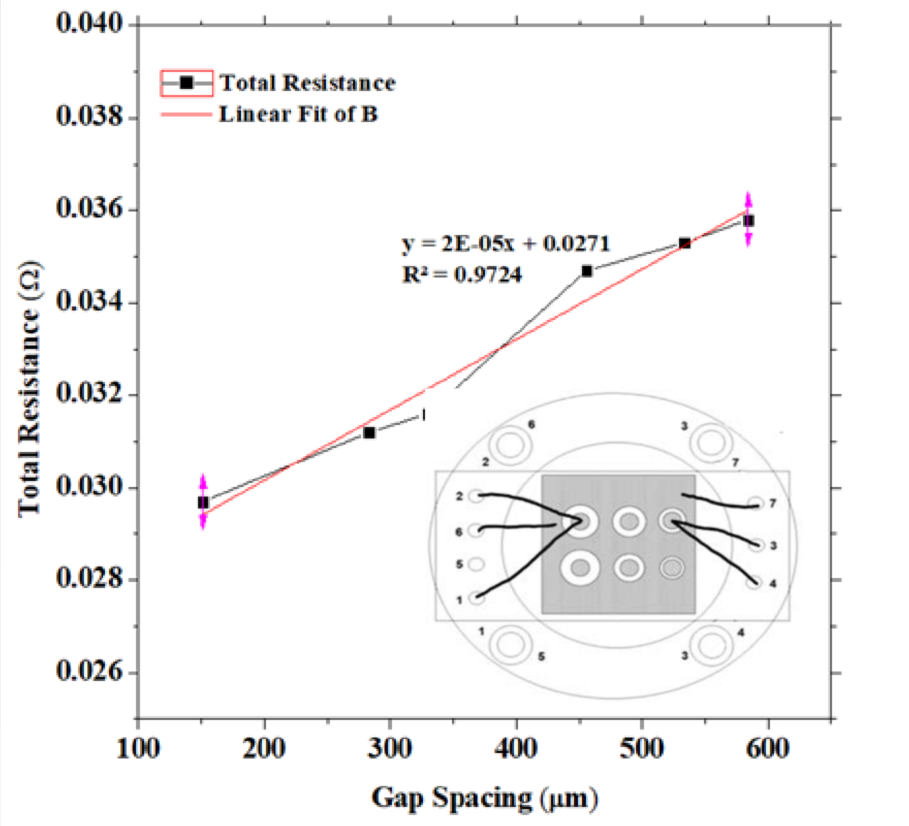

The total resistance versus gap spacing for Heraeus C8710. The contact resistance is the y-axis intercept.

LSM ferromagnetic-paramagnetic transitions

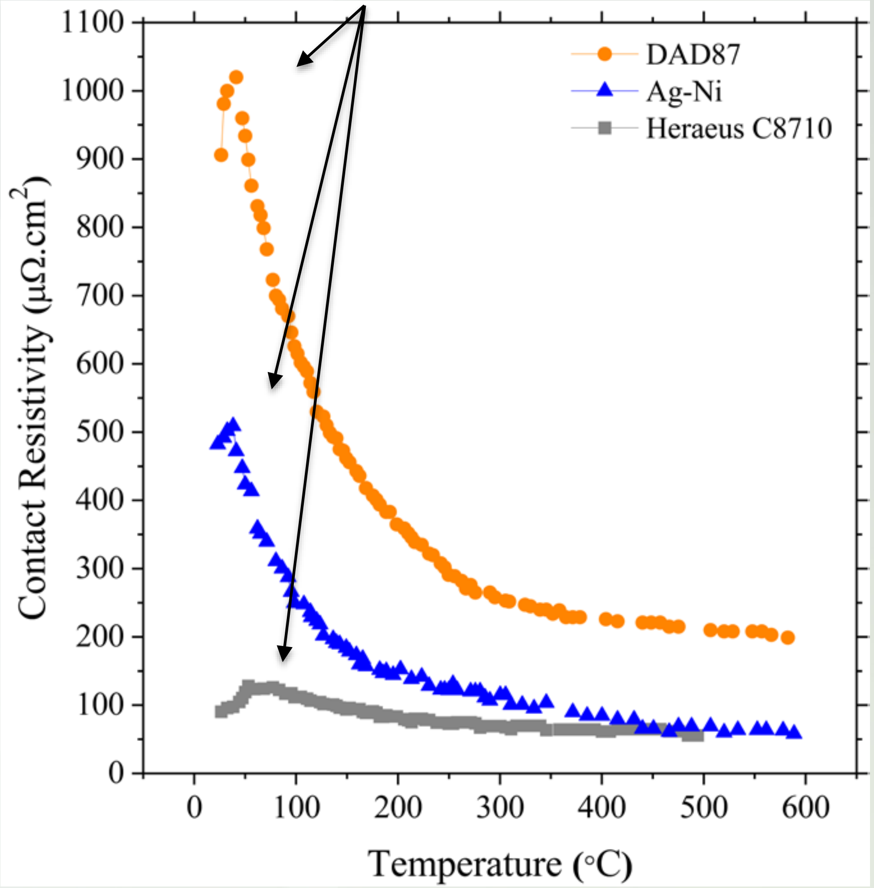

The contact resistivity of 750 °C air annealed Ag circuits at different temperatures

Hammouche, *et al.*, Solid State Ionics(1988)
Hassini, *et al.*, Solid State Sci(2002)

Outline

- **Background and Motivation**
  - Porous Ni Can Promote Ag Wetting on Different Substrates
- **Experiments**
- **Results and Discussion**
  - The Electrical Performance
  - The Mechanical Performance
  - Ag Wetting Molecular Dynamics Simulation and Optimal Pattern Calculation
  - Nickel Phase Sintering Simulation
- **Conclusions**

The Bonding Strength between Ag Pastes and Alumina Was Measured by Tensile Tests

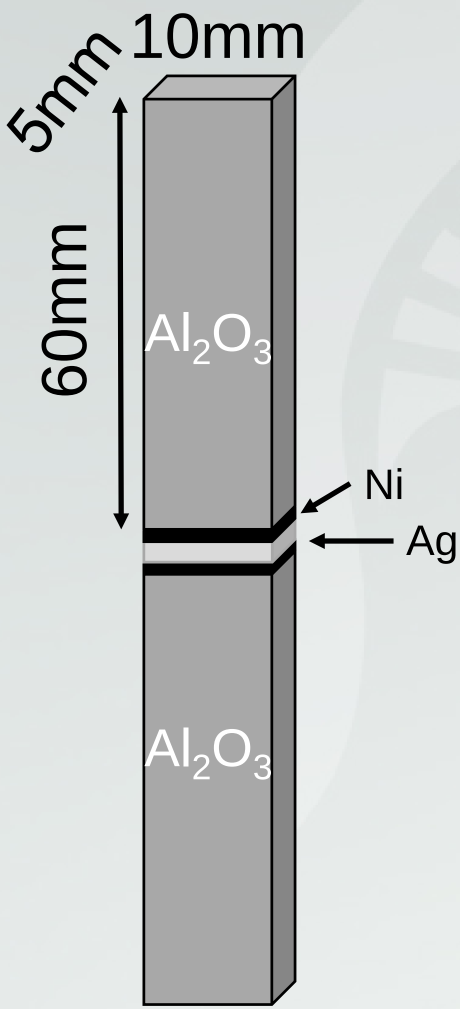

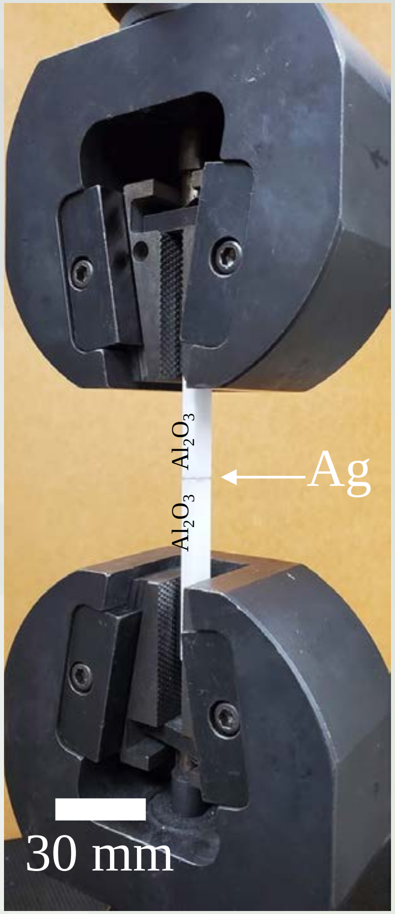

The tensile test sample and experiment set up

Weibull Plots Are a Statistical Approach to Describe Strength Distributions

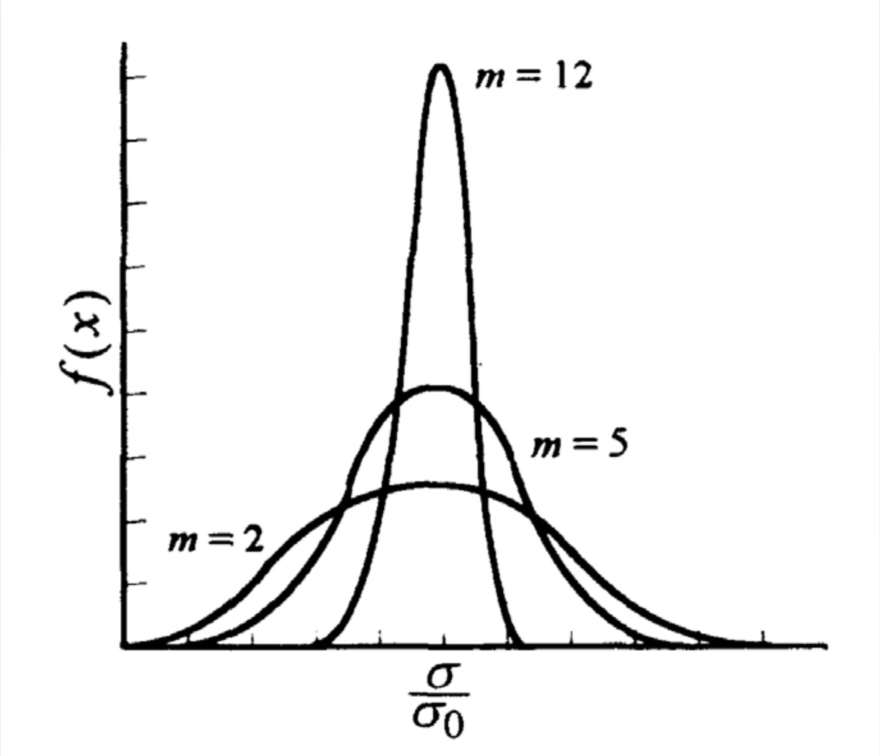

If the survival probability S is assumed to take the form

$$S = \exp[-\left(\frac{\sigma}{\sigma_0}\right)^m]$$

then,

$$\ln\ln\frac{1}{S} = m ln\sigma - m ln\sigma_0$$

where m is a shape factor, referred to as the *Weibull modulus and* σ_0 is the stress where the survival probability is 37%. This last equation indicates that fracture strength data plotted in lnln1/S vs ln σ yields a straight line.

Weibull, W. A Statistical Distribution Function of Wide Applications. **1951,** *103* (730), 293-297.
Barsoum, M. W. *Fundamentals of Ceramics*, Institute of Physics Publishing: Bristol and Philadelphia, 2003.

The Tensile Strength between Ag-Ni and Al_2O_3 Is Stronger than Those of Commercial Ag Pastes

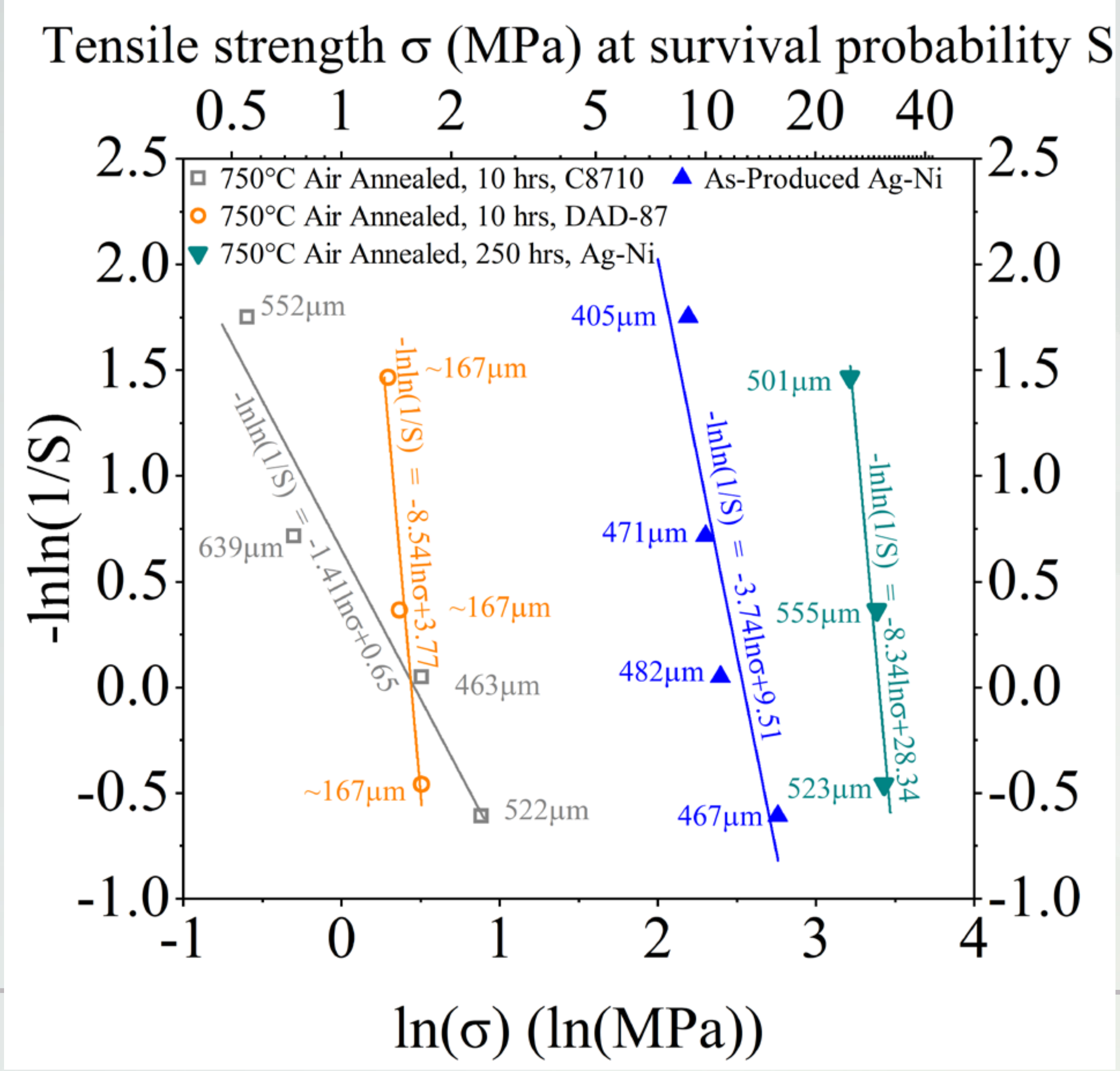

Paste	C8710	DAD-87	Air Annealed Ag-Ni	As-Produced Ag-Ni
Stress (MPa)	6.0×10^{-2}	0.91	3.7	17

Design stress ensuring a survival probability of 99%

Both Ag and Ag-Ni Samples Fractured Along the Metal-Sapphire Interface

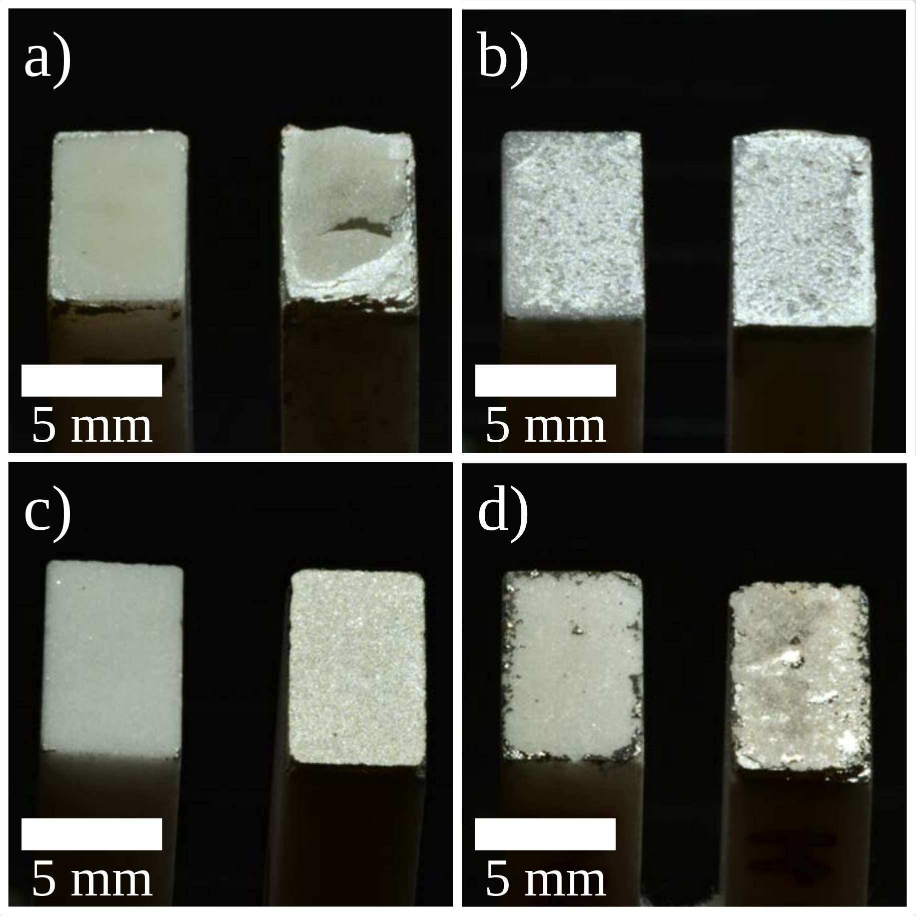

The fracture of (a) air annealed Heraeus C8710, (b) as-produced Ag-Continuous Ni, (c) air annealed Ag-Continuous Ni, (d) air annealed DAD-87

The Sapphire|Ag-Ni Interface Actually Gets Stronger After Oxidation (Even though Brittle NiO is forming)

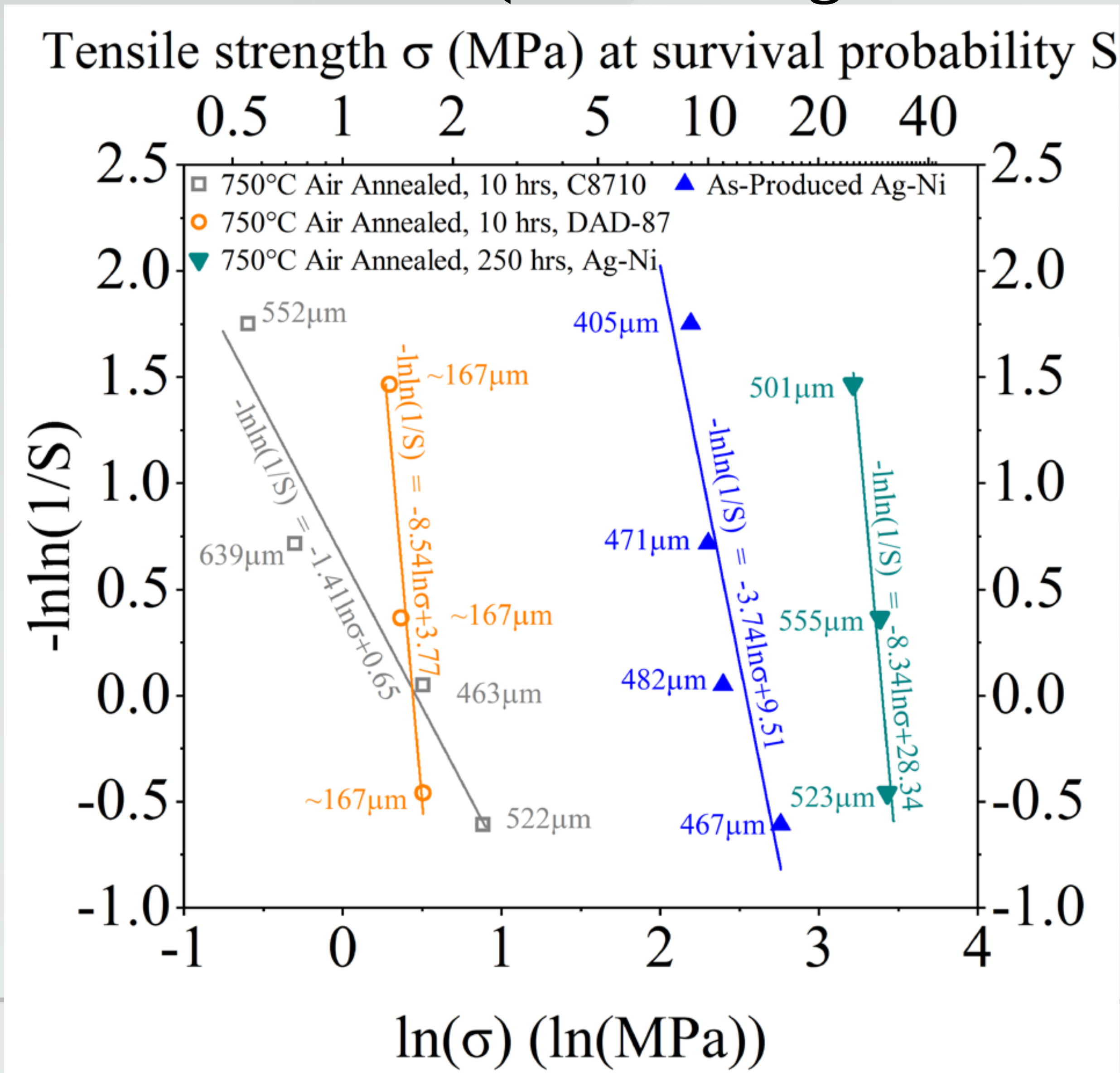

Paste	C8710	DAD-87	Air Annealed Ag-Ni	As-Produced Ag-Ni
Stress (MPa)	6.0×10^{-2}	0.91	3.7	17

Design stress ensuring a survival probability of 99%

More Dissolved Oxygen in the Ag Makes Oxidized Ag-Ni Joints Stronger

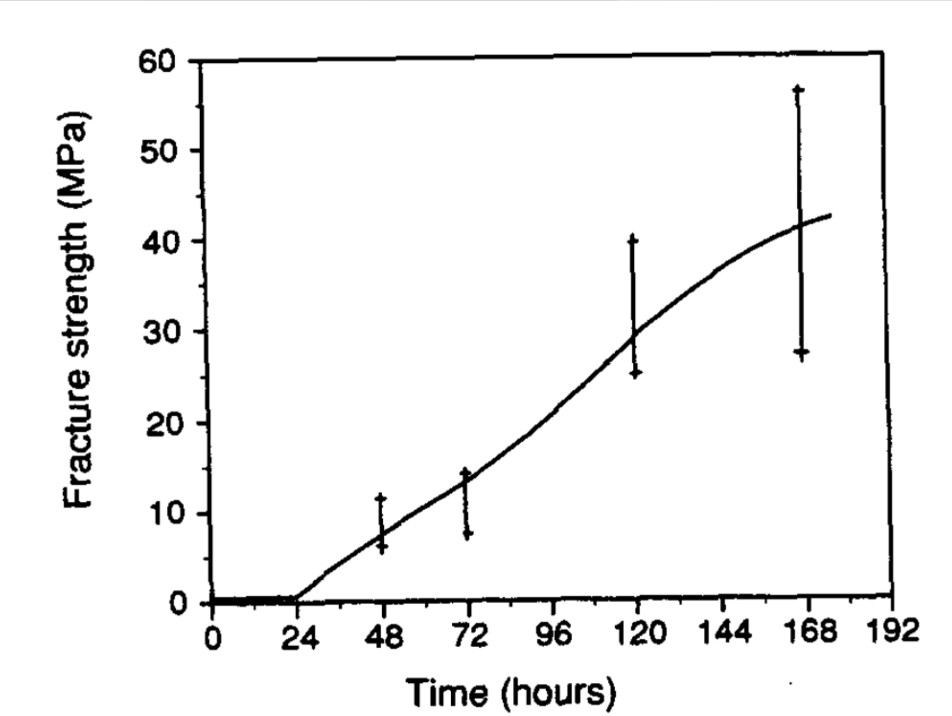

Fracture strength of Ag/Al_2O_3 bonds annealed at 900°C for 24 h in vacuum vs. reoxidation time at 900°C in air

Work of adhesion (J/m^2)	
Ag(l)/YSZ(1 1 1)	(Ag(l)+2O)/YSZ(1 1 1)
0.11±0.01	0.43±0.01

The work of adhesion change between Ag/YSZ substrate with and without oxygen.

Air annealing increased the oxygen concentration in Ag circuits, which increased the work of adhesion and the bonding tensile strength.

Treheux, *et al. Scripta Metallurgica et Materialia;(United States)*(1994)
Phongpreecha, T., *et al.* Acta Materialia(2018)

Outline

- **Background and Motivation**
  - Porous Ni Can Promote Ag Wetting on Different Substrates
- **Experiments**
- **Results and Discussion**
  - The Electrical Performance
  - The Mechanical Performance
  - Ag Wetting Molecular Dynamics Simulation and Optimal Pattern Calculation
  - Nickel Phase Sintering Simulation
- **Conclusions**

Silver-Sapphire, and Silver-Nickel Force Field (FF) Parameters Were Determined by Fitting the Interfacial Binding Energy to Density-Functional Theory (DFT)

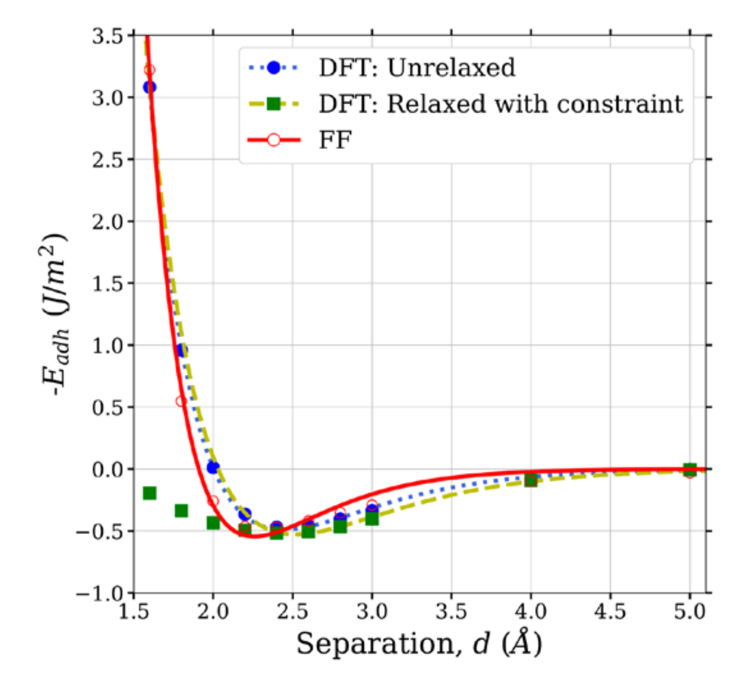

A comparison between the optimized FF and DFT calculations for the interfacial binding energy at various separation distance, d. For the DFT calculations, the unrelaxed interface and relaxed interface with constraint were used. The dotted and solid lines represent fitted UBER curves for each case.

Park *et al*. Enhanced Liquid Metal Wetting on Oxide Surfaces via Patterned Particles. Submitted to *Acta Materialia*. 2020

Molecular Dynamics Simulations Shows that Nickel Promotes the Wetting and Spreading of Silver on Ceramics

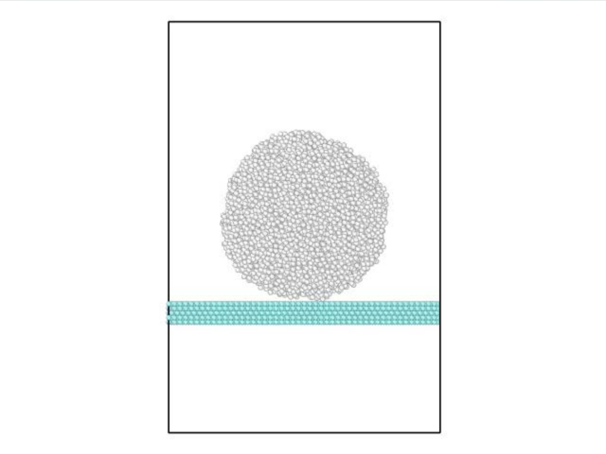

Ag on bare YSZ

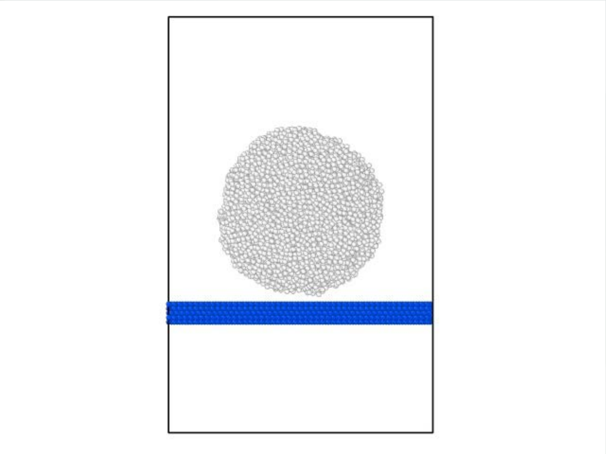

Ag on bare Ni

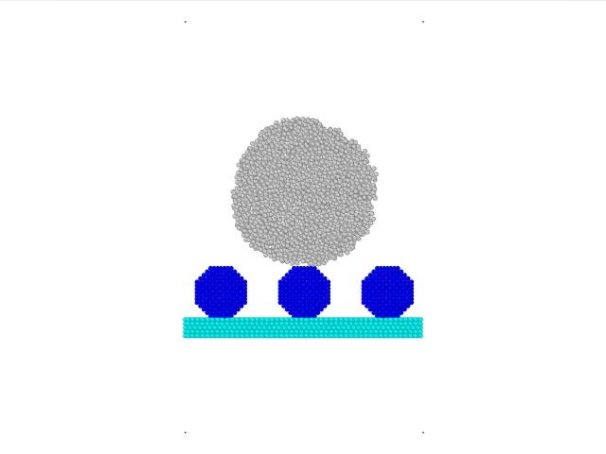

Ag on YSZ with Ni particles

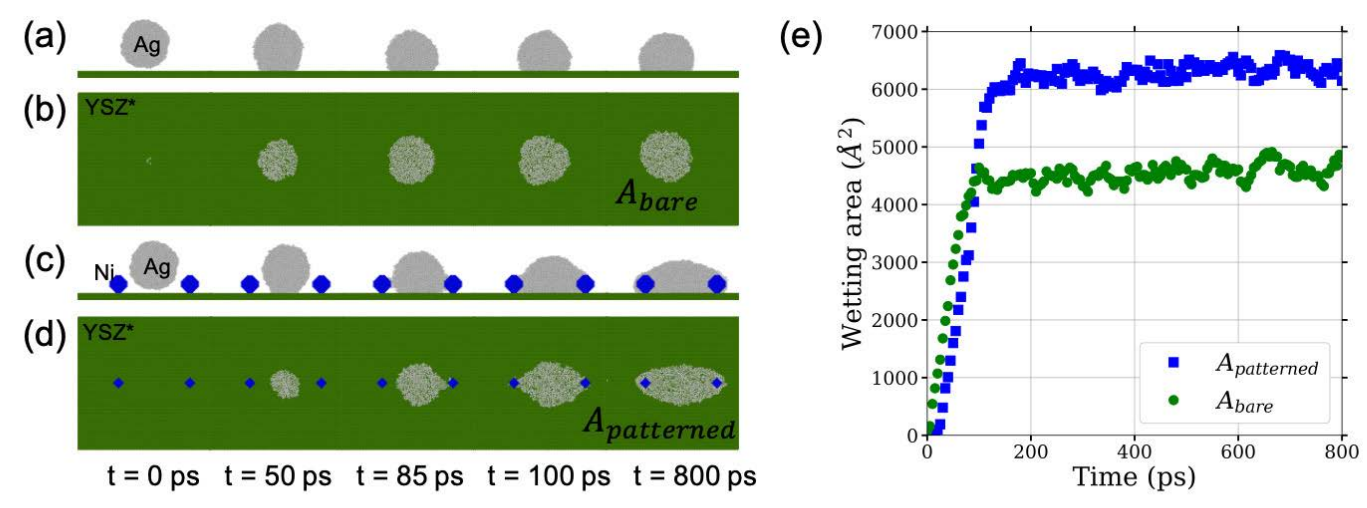

The YSZ area wet by liquid Ag on bare surface from (a) side view and (b) top view; and on Ni patterned surface from (c) side view and (d) top view.

Figure (e) shows the wetting area evolution on two surfaces.

Park *et al*. Enhanced Liquid Metal Wetting on Oxide Surfaces via Patterned Particles. Submitted to *Acta Materialia*. 2020

Hexagonal Ni Particles Patterns Create a Maximum Silver Wetting Area Enhancement of 224%

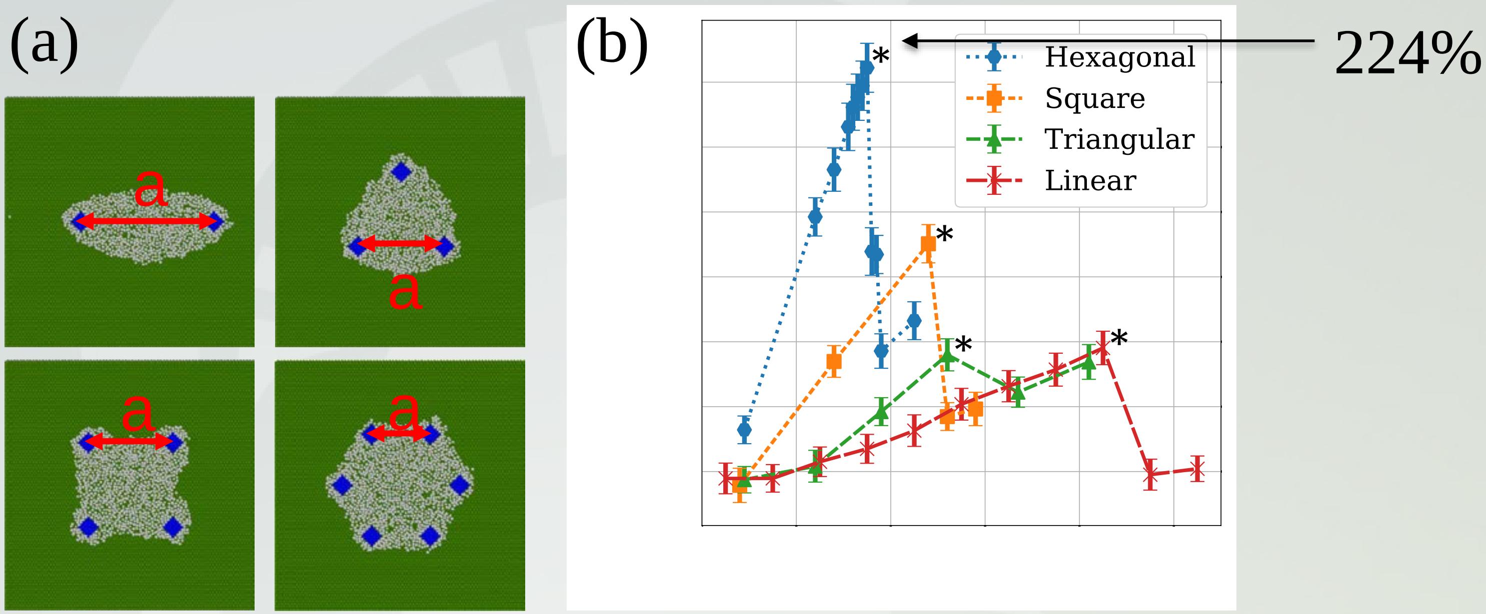

Figure (a): the four different nickel particle configurations on YSZ surface and the wetting area by liquid silver.
Figure (b) the wetting area enhancement by varying the interparticle spacing at each configuration.
Error bars denote the standard deviation of the area enhancement values.

Park *et al*. Enhanced Liquid Metal Wetting on Oxide Surfaces via Patterned Particles. Submitted to *Acta Materialia*. 2020

An Analytical Model Was Established to Analyze the Wetting Enhancement

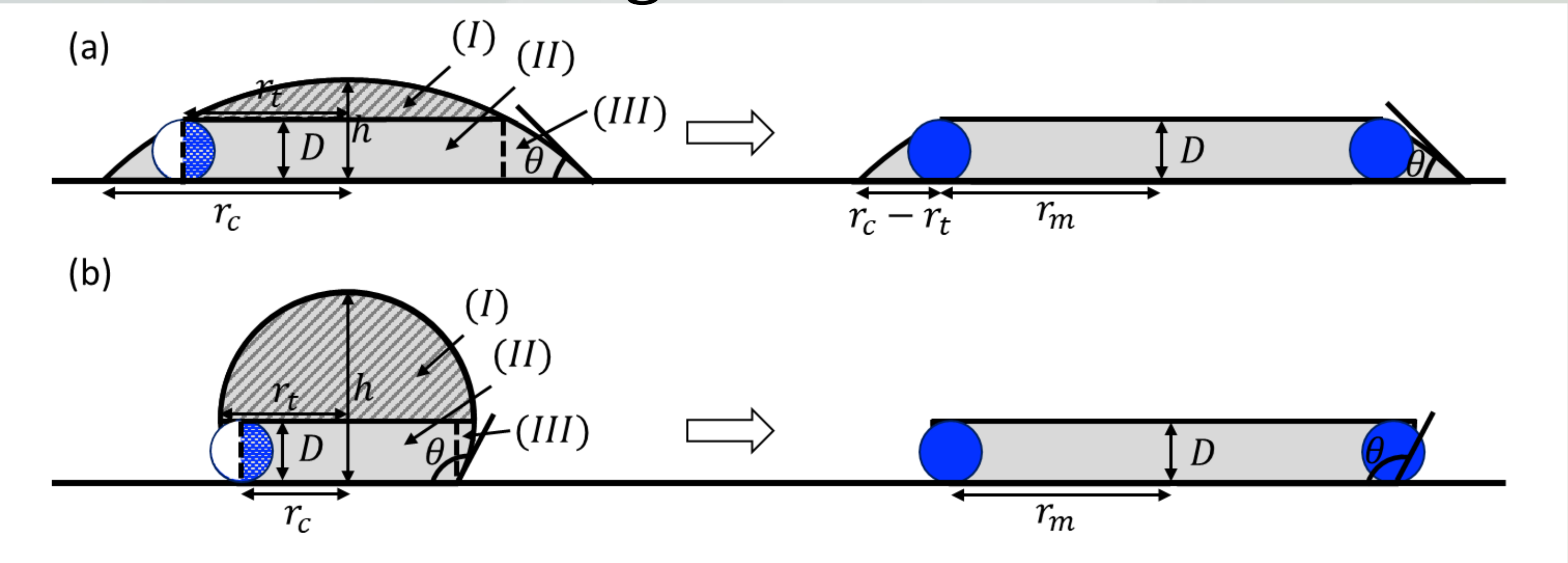

Schematic of the cross-section of a droplet on the substrate, where the shaded gray region represents a Ag liquid droplet on a bare substrate (left), and the cross-section of a transformed droplet when Ni particles (blue circles) are placed on the substrate (right): On the left, the circle refers to a Ni particle to visualize where the Ni particles will be placed for better understanding. The volume of the dotted blue region in the circle was considered to calculate rm. (a) $r_t < r_c$ and (b) $r_t > r_c$.

$$\frac{A_{patterned}}{A_{bare}} = \begin{cases} \dfrac{(r_m + r_c - r_t)^2}{r_c^2} \; for\ r_t < r_c \\ \dfrac{r_m^2}{r_c^2} \; for\ r_t > r_c \end{cases}$$

Park *et al*. Enhanced Liquid Metal Wetting on Oxide Surfaces via Patterned Particles. Submitted to *Acta Materialia*. 2020

The Analytical Model Was Validated by Molecular Dynamics Simulations

Surface	Wetting area enhancement	
	MD	Analytical model
YSZ	2.24 ± 0.076	2.20
Non-Wetting	3.66 ± 0.227	3.76
Large contact angle (<90°)	1.61 ± 0.042	1.49
Small contact angle (<90°)	1.40 ± 0.033	1.32

Park *et al*. Enhanced Liquid Metal Wetting on Oxide Surfaces via Patterned Particles. Submitted to *Acta Materialia*. 2020

Outline

- **Background and Motivation**
  - Porous Ni Can Promote Ag Wetting on Different Substrates
- **Experiments**
- **Results and Discussion**
  - The Electrical Performance
  - The Mechanical Performance
  - Ag Wetting Molecular Dynamics Simulation and Optimal Pattern Calculation
  - Nickel Phase Sintering Simulation
- **Conclusions**

A Three-Dimensional Phase Sintering Model Was Established Based on the Sintered Ni Particle Size Distribution

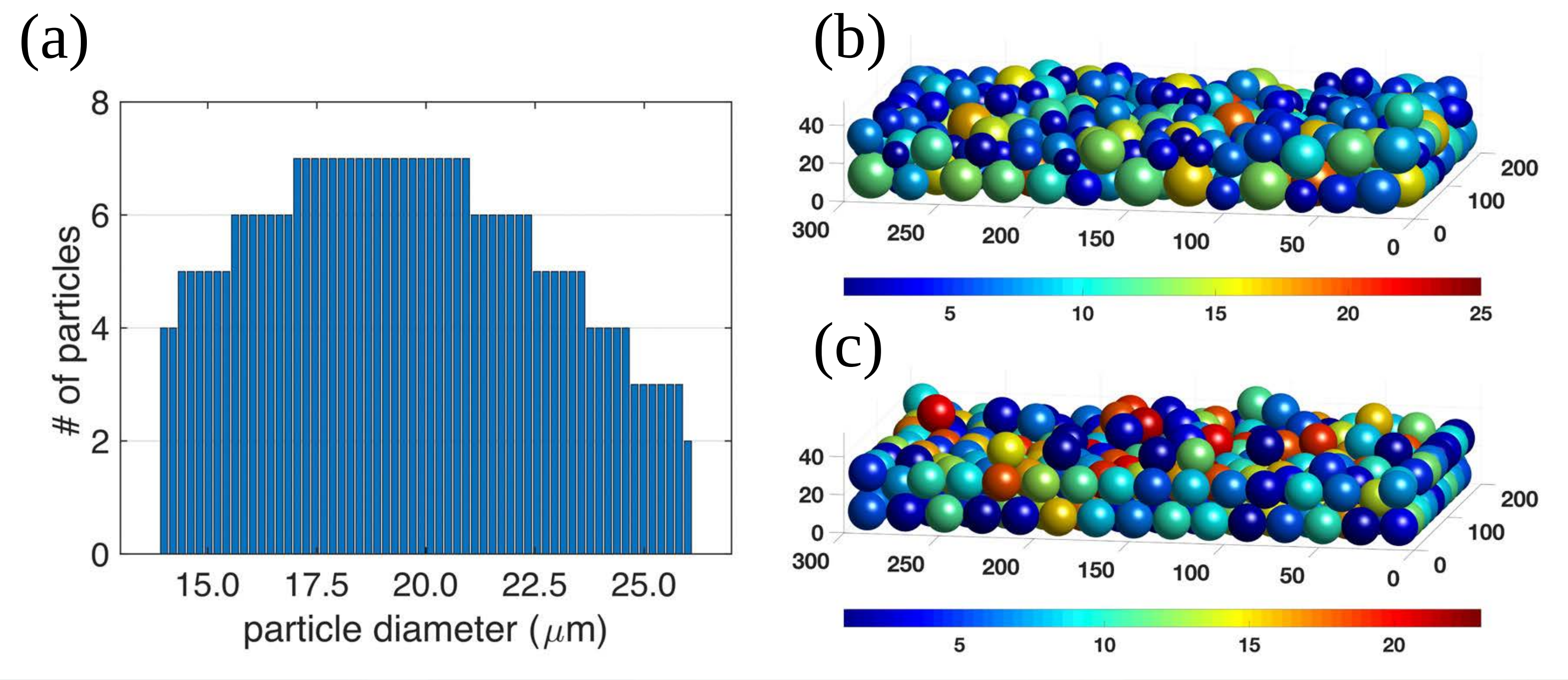

Figure (a): Particle size distribution from sintered nickel scanning electron microscope images. Figure (b): Case 1, Ni particle configuration based on the particle size distribution, which follows a Gaussian curve with lower bound of 14 μm, upper bound of 26 μm and mean at 19 μm. Figure (c): Case 2, Ni particle configuration with a uniform diameter of 20 μm.

Termuhlen *et al*. Three-Dimensional Phase Field Sintering Simulations
Accounting for the Rigid-Body Motion of Individual Grains. In Preparation. 2020

Voids Shrinkage and Volume Densification Were Observed during the Sintering Simulation Process

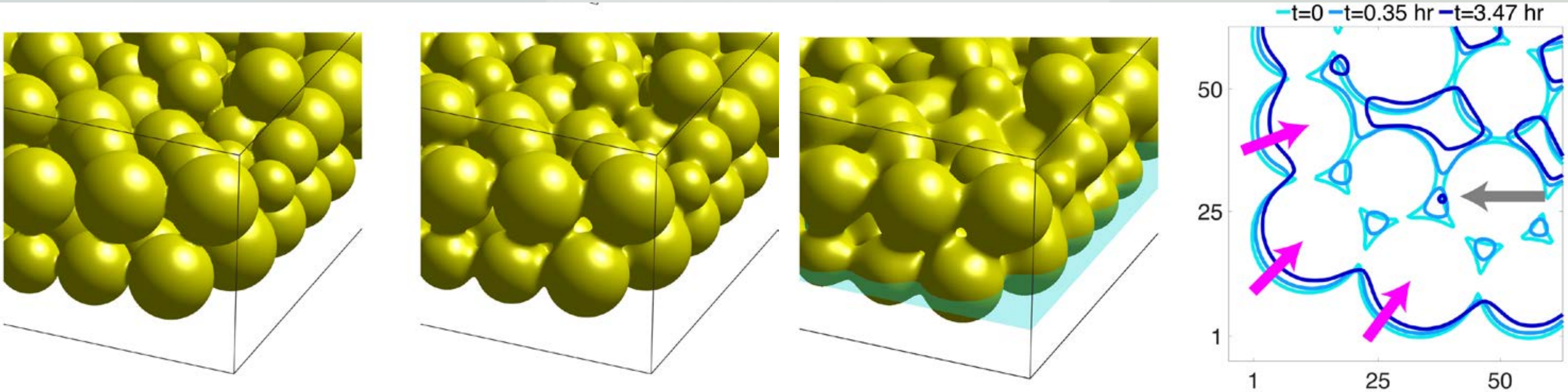

t=0 t=0.35 h t=3.47 h

Ni particles following Gaussian distribution at *t*=0, 0.35h and 3.47h. The contour lines on the z=10 μm plane. Different lines correspond to different time.

Termuhlen *et al*. Three-Dimensional Phase Field Sintering Simulations Accounting for the Rigid-Body Motion of Individual Grains. In Preparation. 2020

The Solid Volume Fraction, Surface Area and Grain Boundary Area Were Calculated During the Sintering Simulation Process

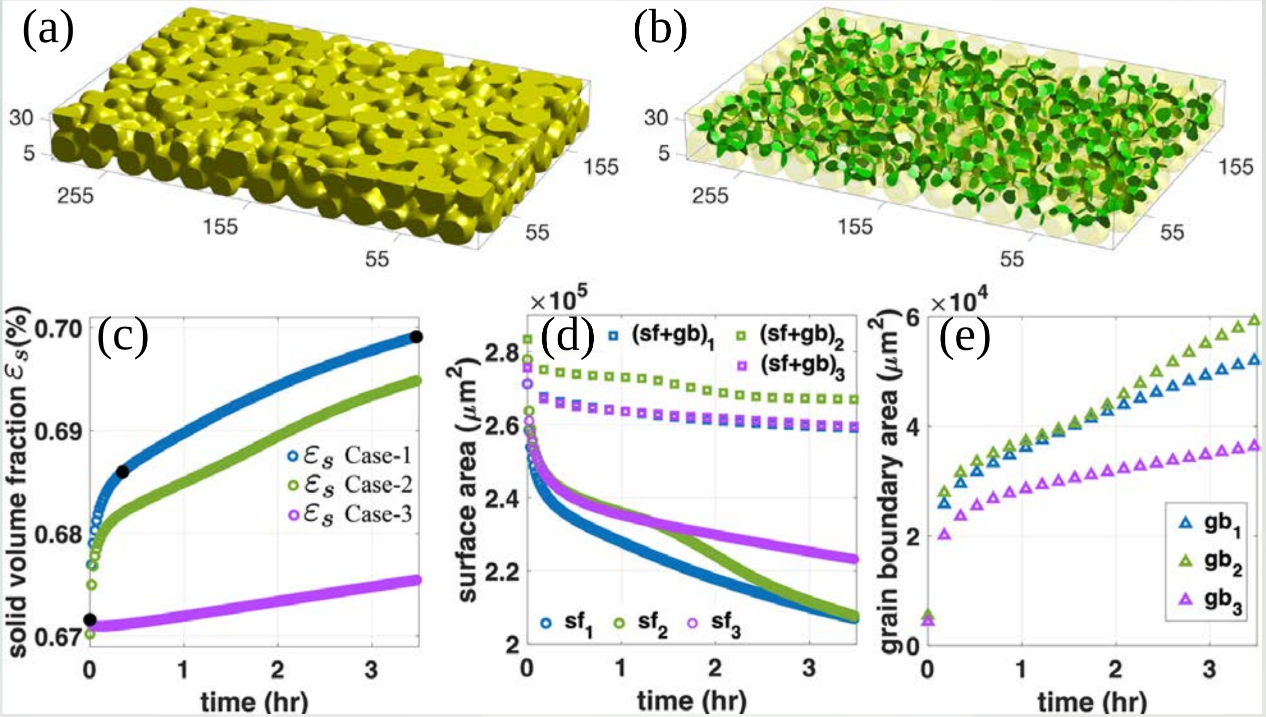

Figure (a): the solid structure at t=3.47 h with Ni particles following Gaussian distribution. (b) the grain boundary in the solid structure shown by green color. (c) the solid volume fraction (Case 3 has identical particle configuration except that rigid-body motion was ignored). (d) the surface area evolution and the sum of surface area and grain boundary (e) the grain boundary area evolution.

The Maximum von Mises Stresses Were Calculated for Each Configuration

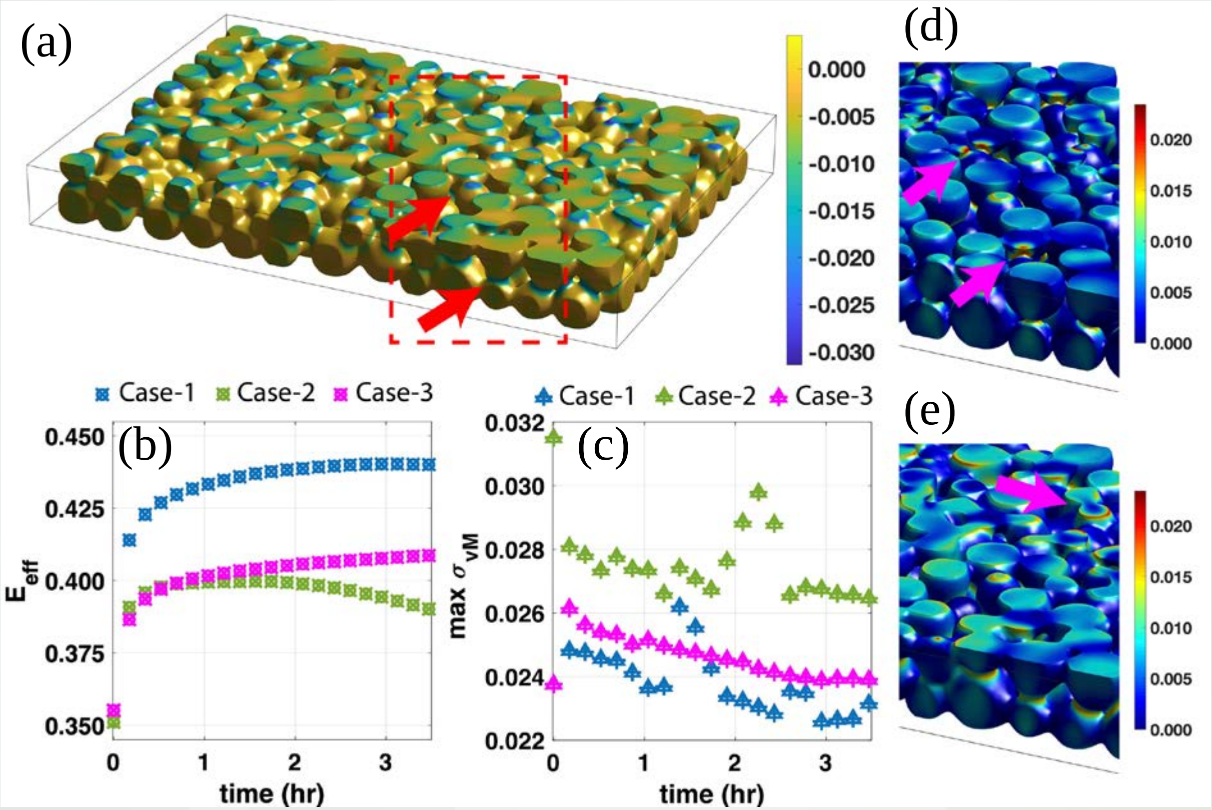

Figure (a): the solid structure at t=3.47 h with Ni particles following Gaussian distribution under the loading of $\bar{\epsilon}_{zz} = -0.01$. (b) The effective Young's modulus of the microstructure at different times. (c) The calculated maximum von Mises stress in the microstructures, where the markers '△' and '+' are for the compression and tension loadings, respectively. The von Mises stress in Case-1 microstructure at (d) t = 0 and (e) t = 3.47 hr, which corresponds to the red box in (a)

Termuhlen *et al*. Three-Dimensional Phase Field Sintering Simulations Accounting for the Rigid-Body Motion of Individual Grains. In Preparation. 2020

Conclusions

1. Here a new Particle Interlayer Directed Wetting and Spreading (PIDWAS) technique was used to produce Ag-Ni circuits on a variety of ceramic substrates that Ag alone would not wet.
2. Ag-Ni circuits have low sheet resistivity.
3. Ag-Ni circuits have a low contact resistivity on LSM.
4. Ag-Ni circuits bond to Al_2O_3 much stronger than commercial Ag pastes. Air annealing enhances their adhesion strength.
5. The optimal hexagonal Ni particle pattern was predicted by molecular dynamics simulation.
6. A porous Phase Field Nickel Sintering model enabling the rigid body motion of individual particles for was established for the first time, allowing an examination in how sintering affects structure-property relations.
7. The PIDWAS technique developed here is one of the few pressureless silver-sapphire joining techniques with a demonstrated capacity for producing dense, intricate, thick film silver patterns on ceramic substrates for circuit, current collector, sealing, joining and other applications.

The Most Common Silver-Sapphire Joining Techniques Comparison

	Constrained Sintering	Pressure Assisted Sintering	Reaction Assisted Sintering	Stress-Migration Bonding	Current Assisted Sintering	Light Assisted Sintering	Pressure Joining	Transient Liquid Brazing	Silver Alloy Brazing	Porous Templated Wetting
Alternative Names / Flavors of this Technique	Pressureless Sintering	Hot Isostatic Pressing, Sintering Forging	In-situ Formation, Reaction Bonding	Silver Direct Bonding	Spark Plasma Sintering, Microwave Sintering	Laser Sintering, Infrared Sintering	Solid State Bonding	Solid Liquid Interdiffusion Bonding, Direct Silver Bonding	Reactive Air Brazing, Active Metal Brazing	THIS WORK
Description	Solid state densification, creep and/or plastic flow induced or assisted by:						Dense Ag foils are deformed and brought into intimate contact with a substrate through the application of an external force	Local melting of a low T_m layer (such as an impurity-induced local eutectic) that is subsequently consumed by reaction with the solid substrate or solid Ag foil	Bulk melting of Ag alloy foils or porous samples with impurities that migrate to the Ag surface to react with the substrate and promote wetting	Bulk melting and subsequent wetting and spreading of Ag foils or porous films directed by the placement of Ag-wettable particles on a substrate
	local curvature differences between particles in a porous Ag sample	the application of an external stress to a porous Ag sample	a chemical of physical reaction (such as the reduction of Ag_2O or solvent evaporation to form Ag nano-particles)	Thin film deposition, CTE mismatch, or other internal compress-ional film stresses	Joule heating, electro-migration etc. caused by passing electric current through a porous Ag sample	Joule heating, electro-migration etc. caused by focusing light on a porous Ag sample				
Part Fabrication Temperature	200-550°C [1-4] 750°C-850°C here	250-275°C [5, 6]	90°C [7], 200-400°C [8, 9]	200-300°C [10, 11]	No results for Ag on sapphire	290°C [12] 850°C [13]	260°C with Au|TiW [14], 500-900°C [15, 16]	Additive Dependent , 946°C with Cu [17]	Additive Dependent , 980-1000°C with Cu [18-20]	> 962°C (Ag T_m), 1050°C here
Fabrication Atmosphere	Any	Any	Reaction Dependent	Any	Any	Any	Any	Additive Dependent	Additive Dependent	Additive Dependent
External Fabrication Pressure	0 MPa	1-50 MPa [5, 6, 21]	0 MPa [7], 5-15 MPa [8, 9]	0 MPa	0 MPa	0 MPa	6-7 MPa [14, 15]	0 MPa	0 MPa	0 MPa
Final Ag Relative Density	< 68% [5] 73% here	87% [5]	~85% [7], ~95% [8, 9]	~100% [10, 11]	No results for Ag on sapphire	~70% [12]	~100% [14, 15]	~100% [17]	~100% [18-20]	~100% here
Maximum Joint Tensile Strength	< 3 MPa here	No results for Ag on sapphire	70 MPa [8]	No results for Ag on sapphire	No results for Ag on sapphire	No results for Ag on sapphire	70 MPa [15, 16, 22]	No results for Ag on sapphire	22 MPa with Cu [23] 72 MPa with Cu on Ti [24]	18-35 MPa depending on atmosphere. Likely higher with less Ni

The Most Common Silver-Sapphire Joining Techniques Comparison

	Constrained Sintering	Pressure Assisted Sintering	Reaction Assisted Sintering	Stress-Migration Bonding	Current Assisted Sintering	Light Assisted Sintering	Pressure Joining	Transient Liquid Brazing	Silver Alloy Brazing	Porous Templated Wetting
Maximum Joint Shear Strength	12 MPa [25] 18 MPa [1]	40 MPa [5] 50 MPa [6]	36 MPa [9]	120 MPa [10]	No results for Ag on sapphire	No results for Ag on sapphire	68-75 MPa [22, 26]	No results for Ag on sapphire	90 MPa with Cu [23]	No results for Ag on sapphire
Ag 25^{o}C Sheet Resistivity	2.2 μΩcm here, 5 μΩcm on glass [2] >50μΩcm on Si [4]	2.4 μΩcm [6]	1.6 μΩcm [7]	No results for Ag on sapphire	No results for Ag on sapphire	2.4 μΩcm [13], >8 μΩcm [12]	1.6 μΩcm by virtue of starting with pure, dense, Ag foil	1.6 μΩcm by virtue of having most of the Ag layer be pure, dense, Ag foil	1.9 μΩcm with Cu on lead ziconate titanate [27]	2.2-3.6 μΩcm here, depending on atmosphere.
Maximum Final Ag Use Temperature	Up to ~950^{o}C in air	Up to ~950^{o}C in air	Up to ~950^{o}C in air	Up to ~950^{o}C in air	Up to ~950^{o}C in air	Up to ~950^{o}C in air	Up to ~950^{o}C in air	Depends on the Additive	Depends on the Additive	Up to ~950^{o}C in air, Up to ~1400^{o}C in pO_2 < $1x10^{-5}$
Most Compelling Features for Circuit Production	Easy	Conductive Ag layers produced at low temperature	Conductive Ag layers produced at very low temperature	High adhesion strength	Somewhat reduced sintering temperature	Ability to define circuits with fine line widths	Dense conductive circuits are guaranteed	Adhesion strength can be greater than that of pure Ag	Adhesion strength can be greater than that of pure Ag	Easily made dense, well-adhered thick or thin film Ag circuits
Most Serious Drawbacks for Circuit Production	Low density, poor adhesion, high resistivity	Pressing during fabrication introduces complexity, raises cost, & can crack substrates	Poor adhesion strength is often a problem	Cannot produce thick Ag films on substrates with an arbitrary CTE	Current focusing can cause Ag layer density variations	Poor adhesion. Cannot produce thick film Ag circuits due to laser adsorption	Cannot be used for thin films due to the mechanical fragility of the original Ag foils	Cannot be used for thin films due to the mechanical fragility of the original Ag foils	Better wetting results in less Ag circuit flaws but more chance of molten Ag runout.	High fabrication temperatures and potential atmosphere control raises cost & limits compatible materials

Reference

1. Wang, T., et al., *Low-temperature sintering with nano-silver paste in die-attached interconnection.* Journal of Electronic Materials, 2007. **36**(10): p. 1333-1340.
2. Suganuma, K., et al., *Low-temperature low-pressure die attach with hybrid silver particle paste.* Microelectronics Reliability, 2012. **52**(2): p. 375-380.
3. Stewart, I.E., M. Jun Kim, and B.J. Wiley, *Effect of morphology on the electrical resistivity of silver nanostructure films.* ACS Applied Materials and Interfaces, 2017. **9**(2): p. 1870-1879.
4. Ahn, B.Y., et al., *Omnidirectional printing of flexible, stretchable, and spanning silver microelectrodes.* Science, 2009. **323**(5921): p. 1590-1593.
5. Knoerr, M. and A. Schletz. *Power semiconductor joining through sintering of silver nanoparticles: Evaluation of influence of parameters time, temperature and pressure on density, strength and reliability*. in *2010 6th International Conference on Integrated Power Electronics Systems, CIPS 2010*. 2011.
6. Zhang, Z.Z. and G.Q. Lu, *Pressure-assisted low-temperature sintering of silver paste as an alternative die-attach solution to solder reflow.* IEEE Transactions on Electronics Packaging Manufacturing, 2002. **25**(4): p. 279-283.
7. Walker, S.B. and J.A. Lewis, *Reactive Silver Inks for Patterning High-Conductivity Features at Mild Temperatures.* Journal of the American Chemical Society, 2012. **134**(3): p. 1419-1421.
8. Hirose, A., et al., *A novel metal-to-metal bonding process through in-situ formation of Ag nanoparticles using Ag2O microparticles.* Journal of Physics: Conference Series, 2009. **165**: p. 012074.
9. Asama, K., et al., *Low-temperature metal-to-alumina direct bonding process utilizing redox reaction between silver oxide and organic agent.* Materials Science and Engineering: A, 2017. **702**: p. 398-405.
10. Kunimune, T., et al., *Ultra thermal stability of LED die-attach achieved by pressureless Ag stress-migration bonding at low temperature.* Acta Materialia, 2015. **89**: p. 133-140.
11. Kunimune, T., et al., *Low-temperature pressure-less silver direct bonding.* IEEE Transactions on Components, Packaging and Manufacturing Technology, 2013. **3**(3): p. 363-369.
12. Rahman, K.M.A., D.N. Wells, and M.T. Duignan, *Laser Direct-Write of Materials for Microelectronics Applications.* MRS Proceedings, 2000. **624**: p. 99.

Reference

13. Li, X., et al., *Silver conductor fabrication by laser direct writing on Al2O3 substrate*. Applied Physics A, 2004. **79**(8): p. 1861-1864.
14. Sha, C.-H., et al., *Solid State Bonding of Silver Foils to Metalized Alumina Substrates at 260°C*. Journal of Electronic Packaging, 2011. **133**(4).
15. Serier, B. and D. Treheux, *Silver-alumina solid state bonding: Influence of the work hardening of the metal*. Acta Metallurgica Et Materialia, 1993. **41**(2): p. 369-374.
16. Sérier, B., et al., *Silver-alumina solid state bonding: Study of diffusion and toughness close to the interface*. Journal of the European Ceramic Society, 1993. **12**(5): p. 385-390.
17. Schu¨ler, C.C., et al., *Direct silver bonding – an alternative for substrates in power semiconductor packaging*. Journal of Materials Science: Materials in Electronics, 2000. **11**(5): p. 389-396.
18. Tillmann, W., N.B. Anar, and L. Wojarski, *Mechanical behavior of reactive air brazed (RAB) Crofer 22 APU-Al2O3 joints at ambient temperature*. SN Applied Sciences, 2020. **2**(5): p. 809.
19. Jasim, K.M., et al., *Actively brazed alumina to alumina joints using CuTi, CuZr and eutectic AgCuTi filler alloys*. Ceramics International, 2010. **36**(8): p. 2287-2295.
20. Kim, J.Y., et al., *Effects of atmospheres on bonding characteristics of silver and alumina*. International Journal of Hydrogen Energy, 2008. **33**(14): p. 4001-4011.
21. Lu, G.-Q., G. Lei, and J. Calata, *Nanoscale metal paste for interconnect and method of use* USPTO, Editor. 2008, Virginia Tech Intellectual Properties Inc USA.
22. Treheux, D., et al., *Metal-ceramic solid state bonding: Mechanisms and mechanics*. Scripta Metallurgica et Materialia, 1994. **31**(8): p. 1055-1060.
23. Zhu, M. and D.D.L. Chung, *Improving the strength of brazed joints to alumina by adding carbon fibres*. Journal of Materials Science, 1997. **32**(20): p. 5321-5333.
24. Xin, C., N. Li, and J. Yan, *Microstructural evolution in the braze joint of sapphire to Kovar alloy by Ti-Cu metallization layer*. Journal of Materials Processing Technology, 2017. **248**: p. 115-122.
25. Ogura, H., et al., *Carboxylate-Passivated Silver Nanoparticles and Their Application to Sintered Interconnection: A Replacement for High Temperature Lead-Rich Solders*. Journal of Electronic Materials, 2010. **39**(8): p. 1233-1240.
26. Serier, B., et al., *Experimental analysis of the strength of silver–alumina junction elaborated at solid state bonding*. Materials & Design, 2011. **32**(7): p. 3750-3755.
27. Pavlina, E.J., et al., *Development of silver–metal oxide reactive air braze alloys for electroding PZT ceramics*. Journal of Materials Science, 2007. **42**(2): p. 705-713.